The Cryosphere Discuss., 9, 5373–5411, 2015
www.the-cryosphere-discuss.net/9/5373/2015/
doi:10.5194/tcd-9-5373-2015

The Cryosphere Discussions
Open Access

An investigation of the influence of supraglacial debris on glacier-hydrology

C. L. Fyffe[1], B. W. Brock[2], M. P. Kirkbride[3], D. W. F. Mair[4], N. S. Arnold[5], C. Smiraglia[6], G. Diolaiuti[6], and F. Diotri[7]

[1]Institute of Science and the Environment, University of Worcester, Worcester, UK
[2]Department of Geography, Northumbria University, Newcastle, UK
[3]School of the Environment, University of Dundee, Dundee, UK
[4]School of Geosciences, University of Aberdeen, Aberdeen, UK
[5]Department of Geography, University of Cambridge, Cambridge, UK
[6]Department of Earth Sciences "Ardito Desio", University of Milan, Milan, Italy
[7]Agenzia Regionale per la Protezione dell'Ambiente della Valle d'Aosta, Aosta, Italy

Received: 4 August 2015 – Accepted: 5 September 2015 – Published: 7 October 2015

Correspondence to: C. L. Fyffe (catrionalfyffe@live.com)

Published by Copernicus Publications on behalf of the European Geosciences Union.

Abstract

The influence of supraglacial debris on the rate and spatial distribution of glacier surface melt is well established, but its potential impact on the structure and evolution of the drainage system of extensively debris-covered glaciers has not been previously investigated. Forty-eight dye injections were conducted on Miage Glacier, Italian Alps, throughout the 2010 and 2011 ablation seasons. An efficient conduit system emanates from moulins in the mid-part of the glacier, which are downstream of a high melt area of dirty ice and patchy debris. High melt rates and runoff concentration by intermoraine troughs encourages the early-season development of a channelized system downstream of this area. Conversely, the drainage system beneath the continuously debris-covered lower ablation area is generally inefficient, with multi-peaked traces suggesting a distributed network, which likely feeds into the conduit system fed by the upglacier moulins. Drainage efficiency from the debris-covered area increased over the season but trace flow velocity remained lower than from the upper glacier moulins. Low and less-peaked melt inputs combined with the hummocky topography of the debris-covered area inhibits the formation of an efficient drainage network. These findings are relevant to regions with extensive glacial debris cover and where debris cover is expanding.

1 Introduction

Debris-covered glaciers are prevalent in mountainous regions such as the Pamirs and Himalaya (Scherler et al., 2011; Bolch et al., 2012), Caucasus Mountains, Russia (Stokes et al., 2007), and the Western Alps (Deline et al., 2012) and the extent and thickness of debris-cover on glaciers is increasing in many regions (Bolch et al., 2008; Bhambri et al., 2011; Lambrecht et al., 2011; Kirkbride and Deline, 2013). Glacier-runoff is important for downstream water resources, especially during dry seasons (Xu et al., 2009; Maurya et al., 2011). The ablation of ice has a non-linear relationship to the

TCD
9, 5373–5411, 2015

thickness of the overlying debris, with the exact relationship determined by the debris thermal and radiative properties. The relationship between ablation and debris thickness has been derived for several different glaciers and surface covers (e.g. Østrem, 1959; Mattson et al., 1993; Kirkbride and Dugmore, 2003). The dominant effect is a reduction in the melt rate compared with that of bare ice where debris is continuous and more than a few centimetres thick (Brock et al., 2010), with recent hourly energy balance modelling suggesting the debris causes attenuation of the diurnal melt signal (Fyffe et al., 2014).

On debris-free temperate glaciers, dye-tracing studies have demonstrated that the seasonal evolution of the hydrological system, characterised by increasing efficiency over time, is closely linked to the increase in volume and daily amplitude of surface meltwater inputs associated with the upglacier retreat of the seasonal snowline (Nienow et al., 1998; Willis et al., 2002; Campbell et al., 2006). Understanding the nature and evolution of the glacial drainage system is important because it controls how meltwater inputs impact glacial dynamics (Mair et al., 2002), with the glacial dynamic response affecting erosion rates (Hallet et al., 1996). However, only Hasnain et al. (2001) have carried out dye tracing on a debris-covered glacier, focussing on the autumn close-down rather than the spring evolution of the hydrological system, and not dealing explicitly with the influence of debris cover. Direct investigation of englacial conduit systems within debris-covered glaciers (e.g. Gulley and Benn, 2007) have not yet revealed the morphology of inaccessible regions, or gauged the efficiency of the entire system. Considering the strong influence debris has on surface ablation rates (Nicholson and Benn, 2006; Lejeune et al., 2013; Fyffe et al., 2014) extensive debris cover can be expected to influence the morphology and evolution of a glacier's hydrological system, but the nature and extent of this impact is not currently known. Based on field investigations at an alpine debris-covered glacier, this study therefore has two aims:

1. to understand the influence of debris cover on the daily amplitude and magnitude of surface meltwater input to the glacial drainage system;

TCD
9, 5373–5411, 2015

2. to determine the morphology and seasonal evolution of the englacial and subglacial hydrological system and its relationship to the spatial distribution of supraglacial debris cover.

2 Study site

Miage Glacier is situated in the Western Italian Alps (Fig. 1). It originates from four main tributaries, the Mont Blanc, Dome, Bionassay and Tête Carrée Glaciers, which form steep icefalls prior to joining the main tongue. As the main tongue enters Val Veny it bends eastwards before splitting into the large northern and southern lobes and smaller central lobe. The glacier area is 10.5 km^2 over an elevation range of 1740 to 4640 m a.s.l. The lower 5 km of the glacier is completely covered by debris which averages 0.25 m in thickness (Foster et al., 2012), except for isolated debris-free ice cliffs (Reid and Brock, 2014). The debris increases in thickness with distance down glacier so that over most of the lower tongue it is thicker than the "critical thickness" (see Kirkbride and Dugmore, 2003), resulting in reduced ablation compared to bare ice. At higher elevations (above c. 2500 m a.s.l.) the debris is confined to medial and lateral moraines with the intervening ice having a patchy covering of dust to boulder sized sediment (hereafter "dirty ice"). The debris originates predominantly from rockfalls and mixed snow and rock avalanches from the steep valley sides (Deline, 2009). Diolaiuti et al. (2009) found that the debris cover, and its influence on ablation, strongly influenced changes in the glacier's volume over time. A distributed surface energy-balance melt model for the glacier was recently developed by the authors and used to explore patterns and rates of surface melting (Fyffe et al., 2014).

TCD
9, 5373–5411, 2015

3 Methods

3.1 Runoff

3.1.1 Proglacial runoff

Field data were collected at Miage Glacier over two ablation seasons, from 5 June 2010 to 13 September 2010, and from 4 June 2011 to 16 September 2011.

The main outflow stream from the glacier exits the northern lobe, while very little drainage exits the southern lobe. Discharge was monitored at a gauging station directly downstream of the northern portal (Fig. 1). Stage was measured using a pressure transducer mounted in a well attached to a large, stable boulder (see Table 1 for details). The Onset HOBO pressure data were compensated using air pressure data from Mont de la Saxe, 7.6 km from the gauging station. A high flow event in June 2011 caused damage to the well, resulting in lost data between 18 June 2011 and 3 August 2011 and the repositioning of the well. Other data voids are 27 to 28 August 2010 and 4 to 8 September 2010. All recorded stages were adjusted to the datum of the June 2010 stilling well so that a single stage-discharge rating could be applied to the entire record. The stage-discharge rating was derived from discharges calculated from dye dilution gauging using rhodamine WT. In total 16 dye dilution gaugings provided a two-part rating curve which has a standard error of the estimate of 0.76 $m^3 s^{-1}$, which gave a percentage error of 14.6 % using the average daily discharge in 2010 of 5.37 $m^3 s^{-1}$.

3.1.2 Supraglacial stream measurements

Prior to conducting a dye trace, the discharge and velocity of the chosen supraglacial stream (Q_s and u_s, respectively) were measured in 2011. Either the velocity-area method or salt dilution gauging was used to measure supraglacial stream discharge. Dilution gauging was preferred, but this was not always possible. Surface velocity was

TCD
9, 5373–5411, 2015

measured using floats, which are likely to overestimate mean depth-averaged velocity (Dingman, 2002). Floats usually followed the stream thalweg and so travelled faster than the width and depth-averaged flow. The salt dilution gauging was performed using a portable conductivity probe (Table 1).

The dilution gauging velocity is the distance between injection and detection points divided by the time between injection and peak of the concentration curve. This gives the average water velocity, a preferable measure of velocity than the float method. Therefore, discharges measured using the velocity-area method were adjusted using the ratio of dilution to float velocity found from simultaneous measurements.

3.2 Delimiting supraglacial catchments and routing

Supraglacial streams and their catchments were defined by applying Arnold (2010)'s lake and catchment identification algorithm (LCIA) to a digital elevation model (DEM). The algorithm calculates surface slope and direction of steepest descent (flow direction) for each cell. Sinks (potential lakes) are defined as cells with no lower neighbours, with the algorithm using the flow direction matrix to find the upstream cells that feed to that sink. The catchment outlet is determined as the lowest cell on the catchment boundary, with each cell lower than this within the catchment flooded with water to identify lakes. The algorithm also determines the flow pathways between each catchment allowing the entire supraglacial stream and lake network to be defined. This supraglacial algorithm is favoured over most others because it does not rely on the artificial filling of sinks before calculating the flow routing. Arnold (2010) provides detailed model methods. The DEM was derived from airborne LiDAR surveys in 2008 (provided by Regione Autonoma Valle d'Aosta, VDA DEM hereafter) and has a spatial resolution of 2 m and a vertical accuracy of < 0.5 m. The VDA DEM was resampled to a 4 m cell size and was clipped to the glacier catchment boundary which follows the mountain ridge surrounding the glacier and the moraine crests outside of the glacial trough.

TCD
9, 5373–5411, 2015

3.3 Ice thickness

Ice thickness data was required to calculate the conduit closure rates (see Appendix). The ice thickness is calculated as the difference between the surface and bed elevation. The VDA DEM was used to give the surface topography. A map of the bed topography in Deline (2002) (based on Carabelli, 1961; Casati, 1998; Lesca, 1974), was scanned, georeferenced, digitised and interpolated into a raster with a 25 m cell size. Unfortunately, the resolution of the map contours was low and the fit of the map to the glacier outline was poor due to a lack of clear control points. Resulting conduit closure rates should therefore be treated with caution.

3.4 Meteorological stations

Three meteorological stations were located on the glacier. The lower and upper weather stations (LWS and UWS hereafter) were full energy-balance stations situated on continuous debris cover, with the ice weather station (IWS) measuring only air temperature on an area of dirty ice (Fig. 1). Details of the instruments installed on LWS, UWS and IWS are given in Brock et al. (2010) and Fyffe et al. (2014).

3.5 Dye tracing

In total 48 dye injections were conducted into 16 surface streams. All dye traces were carried out using 21 % rhodamine WT liquid dye. Between 40 and 280 mL of dye was used per injection. The dye trace was detected at the gauging station using a fluorometer (see Table 1) recorded by a Campbell logger (CR500, until 14 June 2011 when it was replaced with a CR10X) at either 5 or 1 min intervals. Each fluorometer was calibrated in the field for each dye lot.

Although it was intended to use injection points which led directly into a moulin, this often was not possible, especially where debris cover was thick. Streams often flow beneath the debris, making it difficult to inject dye. In some cases, difficulty in

TCD
9, 5373–5411, 2015

accessing moulins due to ice cliffs meant an injection point was used further upstream. During 2011 the execution of repeat injections at individual points was emphasised. Five injection points were chosen, two on the lower glacier debris zone (S5 and S7), and three on the upper glacier debris zone (S12, S14 and S15) (see Fig. 1). The three upper points were intended to be spread equally along the glacier, but following an extensive search the only moulins found were all in a relatively small area. The parameters calculated for each dye-breakthrough curve are given in Table 2.

The injection point into S5 was into a stream 446 m upstream of the moulin and so the trace flow velocity (u) was adjusted to account for the time spent in the supraglacial stream, using the measured supraglacial stream velocity (u_s) at the time of the test (2011 only). Henceforth, only adjusted u is given.

4 Results

4.1 Meteorological and snow cover conditions

An overview of the air temperature, discharge and precipitation in both years is given in Fig. 2. On average, air temperatures in the June to August period were similar in 2010 and 2011 (11.1 and 10.5 °C, respectively). June was relatively cool in both years; although a rise in air temperature along with heavy rainfall resulted in a significant increase in discharge on 18 June 2011. In early June 2010 snow cover was continuous above 2290 m a.s.l. (close to S9). In contrast, the continuously debris-covered zone was mainly snow free in early June 2011, with continuous snow cover only above 2400 m a.s.l., due to prolonged high temperatures in May (Fig. 2b). Clean ice was exposed in places on the main tongue, above the Dome Glacier confluence. July 2010 was warmer than July 2011 (mean air temperatures were 13.1 and 9.4 °C, respectively) whereas August was cooler in 2010 than in 2011, (mean air temperature 10.5 and 12.6 °C, respectively).

TCD
9, 5373–5411, 2015

4.2 Supraglacial hydrology

The mean Q_s and u_s for each of the 2011 streams is given in Table 3, with values for each injection time in Table 5. S14 (the main stream draining the western side of the upper glacier, Fig. 3c) and S15 (the main stream draining the eastern side of the upper glacier, Fig. 3b) had the highest Q_s and u_s of those measured. They had relatively large catchments bounded laterally by the central and lateral moraine crests (Figs. 4 and 5). Supraglacial streams were difficult to find on the continuously debris-covered zone, and there was a lack of well-defined moulins. Streams cut laterally into the ice, forming ice cliffs from which the debris collapses; hiding the stream beneath the boulders. S5 (the largest stream observed on the lower glacier) and S7 both had relatively low Q_s and u_s. Figure 5 clearly shows that on the lower glacier catchment sizes are smaller and no-longer controlled by the lateral moraines.

4.3 Englacial and subglacial hydrology

Dye trace parameters for all 2010 and 2011 injections are reported in Tables 4 and 5, with dye return curves shown in Figs. 6 and 7. For ease of reference, injections into S9 and above will be termed upper glacier traces (zone of patchy debris and bare ice), while those into S8 and below will be termed lower glacier traces (continuously debris-covered ice).

4.3.1 Spatial patterns

Generally, the water entering the glacier via the main moulins around the upper limit of continuous debris cover travelled quickly to the proglacial stream, with mean u of the upper glacier traces (S10–S15) being $0.56\,\mathrm{m\,s^{-1}}$. These traces also generally had single peaked return curves (Figs. 6a and 7d–f) and relatively high percentage dye returns (P_r), confirming that the majority of the water was routed efficiently. Most streams from the lower glacier had low u (the average for all lower glacier injection points was

TCD
9, 5373–5411, 2015

0.26 m s^{-1}), with the exception of S6 and S8 (Figs. 3a and 6a) which had a faster u of 0.58 and 0.43 m s^{-1}, respectively. However, generally meltwater produced on the upper glacier could reach the proglacial stream before meltwater produced at the same time on the lower glacier. Return curves from lower glacier traces were generally broader and several displayed multiple peaks (Figs. 6b and 7a–c).

A striking result is that average u increases with distance upglacier and is significantly positively correlated with the distance from the gauging station, (p value = 0.005, Pearson's r = 0.709) (Fig. 8a). P_r was also significantly positively correlated with distance from the gauging station (Fig. 8b, p value = 0.032, Pearson's r = 0.620, excluding P_r values greater than 100 %). The average P_r for injection points below and including S10 was always less than 48 % with an average of 38 %, while for injection points S11 and above the average P_r was at least 50 % with an average of 63 %.

4.3.2 Seasonal evolution

Lower glacier

Lower glacier traces in early June were generally slow (e.g. traces into S1, S3, S5 and S7 had $u < 0.2$ m s^{-1}) and often displayed multiple peaks (e.g. S5_060611 and S7_050611, Fig. 7b and c). The shape of the S5 dye breakthrough curve changed from six to three more prominent peaks between 6 and 12 June 2011 (Fig. 7b) despite u remaining at 0.07 m s^{-1}. Similarly, there was a change between S7_050611 and S7_110611 from a multi-peaked return curve to a curve with one steeply-rising main peak (Fig. 7c).

Between June and July 2011 u at S5 increased substantially, the dispersion coefficient (D) and dispersivity (b) decreased markedly and P_r increased, even though the July input discharge was similar to June. The shape of the dye breakthrough curve changed to a steeply rising main peak, with a later secondary peak (Fig. 7b), similar to the trace shape and P_r at the same stage in 2010 (S5_300710, Fig. 7b). The

TCD
9, 5373–5411, 2015

S3_290710 trace produced a singular peak, much clearer than its June counterpart, with a faster u and much larger P_r (Fig. 7a).

In September the S3_090910 u was slower than in July but faster than June and had twice the D of the S3_290710 trace (Fig. 7a and Table 4). The S5_120911 trace showed the slowest u of the season and was composed of small peaks before and after a broad main peak (Fig. 7b). Misleadingly, D and b values were the lowest of the season because they were calculated from only the main peak. The form of the trace suggests a complex drainage system composed of a small, fast path, a separate slower but larger path, and a third even slower, small path.

Upper glacier

Most upper glacier traces in June (into S10, S12, S13, S14) had $u > 0.4\,\mathrm{m\,s^{-1}}$, with low D and b, despite the early season stage and extensive snow cover on the upper glacier. Traces tended to give discrete, narrow peaks, although the secondary peak on the S13_110610 trace may suggest temporary water storage in the moulin or a secondary channel (Fig. 6a). The shoulder of the S15_130611 trace (Fig. 7f) might indicate an englacial channel constriction, past which water was released gradually.

Comparing June and July traces, the S15_280711 u was much faster than in June (Fig. 7f) and no longer had a flat top to the trace, causing a reduction in D and b. Conversely, S14 and S12 u was slower than in June, with larger D and b values (13 times larger for S12, Table 5). July input discharges into both moulins were larger than in June. S12, S14 and S15 were all injected again 3 or 4 days later at the start of August. The flow velocities of all three traces were faster than those in late July along with markedly lower D values (Table 5). The channel cross-sectional area (A_m) of all three moulins had also increased since late July. Early August input discharges of S15 and S14 were slightly larger than in July, although for S12 the input discharge was less than half that measured on 30 July 2011. All three breakthrough curves were of single peaks (Fig. 7d–f).

TCD
9, 5373–5411, 2015

The September traces into S12, S14 and S15 showed faster u than the June and end of July traces, but similar, or in the case of S12, slightly slower than their early August traces (Fig. 7d–f and Table 5). D was also greater than in early August, and in the case of S12 and S14 greater than in June.

5 Interpretation and discussion

5.1 The influence of supraglacial debris on glacial topography and hydrology

In the region of the glacier between approximately 2300 and 2500 m a.s.l., surface topography is strongly controlled by contrasting ablation rates between thick moraine-crest debris, and partly debris-covered ice in the intervening troughs, resulting in longitudinal ridges and valleys of 30–40 m vertical amplitude (Fig. 4). Ridge-crest ablation is low at around 0.02 m day^{-1}, compared to 0.05 m day^{-1} in the intermoraine areas, representing the highest ablation rates on the glacier over an extensive area of thin and partial debris cover immediately upglacier from the continuously debris-covered zone (Fyffe et al., 2014). Thus, relatively high discharges of meltwater are focused into the troughs in the mid-part of the glacier, amplifying discharges flowing into the cluster of moulins at S12-S15 (Fig. 5). This explains the relatively large Q_s and u_s measured at S12 and S14 (Sect. 4.2).

Surface relief decreases downglacier due to the gravitational redistribution of debris down moraine flanks into the troughs. This inverts relief development by reversing the ablation gradient down the moraine flanks, reducing the systematic spatial variation in debris thickness, and eventually resulting in the hummocky topography of the lower tongue (Fig. 4). Consequently, there is less potential for the formation of an integrated channel network on the continuously debris-covered zone, resulting in a chaotic, local stream network with hollows which may lead to pond development. Consequently, catchments tend to be smaller than upstream (Fig. 5), demonstrating that continuous debris cover can constrain catchment size. Melt beneath a continuous debris cover is

TCD
9, 5373–5411, 2015

less than that of clean or dirty ice, in 2010 averaging 0.019 m we day^{-1} under continuous cover compared to, 0.025 and 0.047 m we day^{-1} for clean and dirty ice respectively (Fyffe et al., 2014). Therefore, much less meltwater is produced on the lower glacier, despite the lower elevation and warmer air temperatures. This explains the small Q_s and slow u_s of the streams on the lower tongue.

5.2 Establishment of channelized system draining upper glacier surface streams

Fast, peaked and low dispersion dye return traces from the upper glacier indicate that a channelized system connects surface streams originating on clean and dirty ice, above the continuously debris-covered zone, to the proglacial stream. This was the case even in early June 2010 when the glacier was snow-covered well below the elevation of the upper moulins.

It is widely accepted that the seasonal evolution of a temperate glacier's hydrological system is caused by an increase in the magnitude and amplitude of inputs into the system, initiated by the switch from snow to ice melt, which causes pressure fluctuations large enough to destabilise the hydraulically inefficient distributed system into a more efficient discrete channel system (e.g. Nienow et al., 1998; Willis et al., 2002; Campbell et al., 2006). The question of how a channelized network draining the upper glacier moulins could be established prior to the depletion of the winter snow cover could be explained by two factors: (a) the channels did not completely close over the winter; or (b) early season snowmelt inputs were sufficiently large. Both of these possibilities will be evaluated in turn.

Conduit closure calculations estimate that the main conduit system is likely to have closed over the winter (Appendix). Although there is some uncertainty in the ice thickness values, the modelling suggested it would take only 6–9 days for the conduits emanating from S12 and S14 to close, depending upon the ice density and whether they fed into separate or one combined conduit. Furthermore, if the subglacial conduit

TCD
9, 5373–5411, 2015

was broad and low rather than semi-circular (as suggested by the form of the proglacial stream outlet), closure rates would be faster than those estimated (Hooke et al., 1990).

Runoff generated by the large catchment areas supplying the S12 and S14 moulins combined with topographic flow concentration (Sect. 5.1) could produce input discharges large enough to initialise channelization, even from snowmelt. In early June of both years a large supraglacial stream was observed flowing beneath or through the snow cover in the valley to the east of the central moraine above the S12–S14 moulins. The S12–S14 catchments exist at a relatively low elevation (2400–2500 m a.s.l.), below the terminus elevations of most clean glaciers in the western European Alps. Consequently, favourable spring weather conditions could lead to water inputs large enough to destabilise the distributed system. As suggested by Mair et al. (2002), a channelized system could form when a snow pack is still present if the snowpack remains longer into the melt season. This allows time for snowmelt percolation to become rapid enough to develop an efficient supraglacial drainage system at the base of the snowpack, generating input hydrographs with sufficient amplitude to channelize the system.

5.3 Evolution of channelized system over the summer

The u of traces from the upper glacier moulins in 2011 (S12, S14 and S15) remained higher than those from the lower glacier (S5 and S7) throughout the season (Fig. 9a). However, compared to June, the late July return curves S12_300711 and S14_290711 were slower and more dispersed, although they still had singular peaks (Fig. 7d and e, respectively). Surprisingly, this indicates the efficiency of the channel system had reduced since June. In contrast, the early August traces into upper glacier moulins S12, S14 and S15 in 2011 all showed a strong increase in u (Fig. 9a), a decrease in D and b, and an increase in A_m (Fig. 9b), compared to the return curves prior to 31 July 2011.

Normally, it would be expected that increased melt inputs between the early and mid-ablation season would result in a progressively more efficient channel network. The slower and more dispersed July traces could be due to increased conduit roughness, caused by a smaller discharge allowing boulders and cobbles on the conduit

TCD
9, 5373–5411, 2015

floor to decrease flow velocity (Gulley et al., 2012). However June and July proglacial discharges were similar and the degree of dispersion seen was less in June. Rapid changes in flow velocity can also result from inflow modulation and/or changes in the channel geometry (Nienow et al., 1996; Schuler and Fischer, 2009). However similar patterns were observed at three different moulins traced at similar times on different days (Table 5), so it is unlikely that inflow modulation over short time periods was the cause of the differences between the July and August traces. More plausible is that cold weather between 17 and 27 July 2011 (Fig. 2b, maximum daily temperatures were generally below 10 °C, and air temperatures fell below zero at UWS during the mornings of 24 and 25 July 2011) and reduced meltwater inputs resulted in relative closure of the main subglacial conduit (Röthlisberger, 1972). When the weather warmed from 28 July 2011 the system was not able to efficiently evacuate the increased discharges, resulting in hydraulic damming, and the slower u and greater D observed in July. This interpretation is corroborated by an observed increase in glacier sliding velocities over the same period, likely generated by high basal water pressure as water was forced across large areas of the bed (Fyffe, 2012). Conduit diameters likely grew rapidly so that by August the network could accommodate the increased discharges.

The September 2011 traces into the upper glacier moulins (Fig. 7d–f), suggested the drainage system remained more efficient than in late July but slightly less efficient than in early August. Air temperatures remained high throughout August 2011 (mean LWS air temperature in July was 9.4 °C, but 12.6 °C in August 2011), and proglacial discharges were all higher in September 2011 than they were during any earlier traces (Table 5), explaining the preservation of drainage system efficiency. S12b and S14b u in September 2010 was slower than its 2011 counterparts (Fig. 7d and e). Air temperatures during August and September (until 10 September 2011) were much cooler in 2010 compared to 2011 (see Fig. 2). Consequently, input discharges in September 2010 would have been smaller than in 2011, increasing conduit closure rates and slowing water velocities.

TCD
9, 5373–5411, 2015

5.4 Englacial and subglacial drainage beneath continuous debris

The drainage system beneath the continuously debris-covered zone was far less efficient than the upper debris-free area. Traces into S1, S3, S5 and S7 had slower u and in some cases (especially S5 and S7, Fig. 7b and c) displayed multiple peaks, indicating the water spent at least some time within a less efficient hydrological network, with multiple flow paths characteristic of a distributed system. On average, injection points S8 and below had a relatively slow average u of 0.26 m s^{-1}, and a low average P_r of 38 %.

Traces into S3, S5 and S7 showed evidence of drainage system evolution (Fig. 7a–c). Certain peaks of the dye breakthrough curves became more prominent or coalesced over the season, suggesting certain flow paths began to dominate within a more integrated network. Therefore the hydrological network did increase in efficiency, but not to the extent that water was transferred as quickly as from the upper glacier moulins. Later in the season there was evidence that the efficiency of the hydrological network decreased, e.g. a decrease in u and increase in D (S3), or a return to traces with multiple peaks (S5, Fig. 7b), indicating increased flow divergence and the reversion of the system back to the distributed configuration found early in the season.

The role of debris in reducing meltwater inputs below the critical discharge at which channels develop (Hewitt and Fowler, 2008) appears crucial in inhibiting channelisation. Low ablation rates (around 0.02 m we day^{-1}, Fyffe et al., 2014), and an attenuated melt signal under thick debris result in small and likely low amplitude supraglacial stream discharges (Sect. 5.1). Furthermore, the uneven topography of the lower glacier (Figs. 4 and 5) inhibits dendritic drainage system development and results in small supraglacial catchments and consequently smaller but more numerous inputs to the englacial system. These low magnitude and amplitude meltwater inputs can be accommodated within a less efficient glacial drainage system.

These results imply the coexistence of an inefficient drainage system beneath the continuously debris-covered zone with an efficient channelized system which emanates

TCD
9, 5373–5411, 2015

from the upper glacier. Distributed and channelized systems are known to coexist, for instance on Haut Glacier d'Arolla away from the preferential axis of drainage (Nienow et al., 1996), on the western side of Midtalsbreen, southern Norway (Willis et al., 1990), and within the smaller drainage catchment of the South Cascade Glacier, USA (Fountain, 1993), but unusually on Miage Glacier the distributed system occurs downglacier of the channelized network and is the main system of transferring melt on the lower glacier, even though a conduit system exits within the same drainage catchment. However, the proportional distance water has travelled in the efficient and less efficient systems is not known and the systems may not merge until close to the snout.

On the lower glacier it is envisaged that the link between the supraglacial stream and the main subglacial channel is the inefficient part of the system. It is this part which causes the lower u and multi-peaked traces. Borehole experiments at Haut Glacier d'Arolla (Hubbard et al., 1995) revealed an area of distributed drainage adjacent to the main channel which supplied water to, and was the recipient of, water from the main channel, depending upon the direction of the pressure gradient between the two areas. A distributed and channelized system probably occurs simultaneously under Miage Glacier, with the distributed system draining to the main channel system. Unlike the system described by Hubbard et al. (1995), water enters the Miage Glacier distributed system from the surface so it contains water irrespective of the pressure gradient between the channel and distributed system.

Sediment layers are commonly found beneath debris-covered glaciers, due to high rates of sediment supply (Maisch et al., 1999; Hewitt, 2014). It is likely that a layer of sediment underlies the lower glacier (Pavan et al., 1999, cited in Deline, 2002), and if this is thick and highly porous it will likely further inhibit conduit formation, since a sediment wedge downglacier of a hard bed can stall channelisation (Flowers, 2008).

TCD
9, 5373–5411, 2015

6 Conclusions

This is the first extensive investigation of the structure and seasonal evolution of the hydrological system of a debris-covered glacier using dye tracing techniques.

Forty-eight dye injections were conducted into 16 surface streams distributed across both debris-free and debris-covered areas of Miage Glacier over the 2010 and 2011 summers. The return curves were analysed in conjunction with supraglacial stream discharge measurements, meteorological data, proglacial stream discharges and topographical analysis of a DEM. The main findings are that:

1. The upper ablation zone, exhibiting patchy debris cover and high surface melt rates, is connected to the main proglacial stream via an efficient channelized system, which is established early in the season when snow-cover is still extensive, and maintained throughout the ablation season.

2. The majority of meltwater from the lower continuously debris-covered area is drained via an inefficient network which may feed gradually into the main channelized network, although on occasion streams make a direct connection with the main conduit system.

3. Significant and rapid changes in capacity and efficiency of the main channelized network may occur mid-season in response to meltwater supply fluctuations.

4. Although the drainage network beneath the continuously debris-covered zone increased in efficiency between the early and mid-season, it did not become as efficient as the upglacier system.

5. The spatial distribution of debris influences hydrological system development in important and contrasting ways, through its influence on both melt rates and surface topography. First, the establishment and maintenance of an efficient channelized network emanating from moulins draining the upper ablation zone is promoted both by very high ablation rates on patchy debris and dirty ice areas and the

TCD
9, 5373–5411, 2015

topographic concentration of flow into large channels within the moraine troughs. This topographic enhancement is a direct consequence of the large difference in melt rates between medial moraines, which are insulated by thick debris, and the high melt rates of the dirty ice in the intermoraine valleys. Second, the small discharges and low amplitude hydrographs of streams draining the continuously debris-covered area result from both low and attenuated melt peaks beneath thick debris and the hummocky topography which restricts catchment and stream size. This produces dispersed low magnitude melt inputs, preventing water pressure fluctuations becoming great enough to destabilize the distributed system beneath.

These interpretations contrast with conclusions from similar dye tracing studies conducted on debris-free glaciers. In particular, on Miage Glacier: (i) the formation of the channelized network is not related to the position of the snowline and (ii) u increased linearly, rather than decreased with distance upglacier. This means that the hydrological evolution of extensively debris-covered glaciers is distinct from that of clean glaciers.

These findings have implications for those glaciers which are becoming increasingly debris covered (Bolch et al., 2008; Bhambri et al., 2011; Lambrecht et al., 2011) since the debris is likely to influence melt water travel times and therefore the proglacial runoff signal. Debris thickness and spatial extent at Miage Glacier is similar to debris-covered glaciers in mountain ranges such as the Himalayas (Rounce and McKinney, 2014; Schauwecker et al., 2015) and Alaska (Kienholz et al., 2015) hence these findings have relevance to regions where debris-covered glaciers are extensive and common.

Appendix: Conduit closure rates

Conduit closure rates were calculated by integrating Eq. (7) in Hooke (1984, cited in Nienow et al., 1998). The time, t(s) for a conduit to close to a given radius, r_r(m) is given by:

TCD
9, 5373–5411, 2015

$$t = \frac{\ln(r_r) - \ln(r_i)}{\left(\frac{\rho_i g h}{n A_G}\right)^3}, \quad \text{(A1)}$$

where ρ_i is the ice density (kg m^{-3}), g is gravitational acceleration (9.81 m s^{-2}, Oke, 1978), $n = 3$ and $A_G = 5.8 \times 10^{-7}$ Pa s$^{-0.5}$, both constants in Glen's flow law (Nienow et al., 1998). The ice thickness (h, m) was derived from the ice thickness map (see Sect. 3.3) by extracting a profile of thickness measurements (at approximately 25 m intervals) from the proglacial stream portal, up the northern lobe and along the glacier centreline. It was assumed that a single conduit links the upper moulins and proglacial stream, with the initial conduit radius (r_i, m) derived by linearly interpolating the measured input (see below) and proglacial stream discharge, and dividing this by u to give the channel cross sectional area along the entire stream length. The conduit was assumed to be semi-circular and to have effectively closed when it had a radius of 0.01 m.

To understand the sensitivity of the calculations to r_i this was calculated using either the S12, S14 or the sum of the S12 and S14 September 2011 supraglacial discharges. The proglacial discharge was taken as the mean of the proglacial discharge at the injection and peak of the return curve for the respective trace, or the mean for the combined S12 and S14 test. The ice density was also varied from 830 kg m^{-3} (lowest density of glacial ice, Paterson, 1994) to 920 kg m^{-3} (pure ice at 0 °C, Oke, 1978).

In all simulations the largest distance from the gauging station at which the conduits would take 4 months to close was between 1820 and 1844 m, around 3 km downglacier of S12 and S14. It was calculated that the ice would need to be 144 to 160 m thick (depending upon the ice density) in order for a combined S12 and S14 conduit to take 4 months to close, whereas the ice thickness calculated using the 2008 DEM at the elevation of the S12 and S14 moulins was 375 to 380 m.

TCD
9, 5373–5411, 2015

Acknowledgements. This work was performed while C. Fyffe was in receipt of a studentship from the School of the Environment, University of Dundee. The authors thank the University of Worcester for kindly funding the publication of this paper. The authors would like to thank J. Holden for the loan of a Seapoint Rhodamine fluorometer and P. Nienow for advice on performing dye tracing studies. F. Brunier from Regione Autonoma Valle d'Aosta kindly provided air pressure data from Mont de la Saxe. Students from the University of Dundee, Northumbria University, Aberdeen University and Cambridge University as well as L. Gilbert provided invaluable help in the field. We would also like to thank M. Vagliasindi and J. P. Fosson of Fondazione Montagna Sicura for excellent logistical support at the field site. The VDA DEM was kindly provided by Regione Autonoma Valle d'Aosta (Modello Altimetrico Digitale della Regione Autonoma Valle d'Aosta aut. n. 1156 del 28 August 2007).

References

Arnold, N. S.: A new approach for dealing with depressions in digital elevation models when calculating flow accumulation values, Prog. Phys. Geogr., 34, 781–809, 2010.

Bhambri, R., Bolch, T., Chaujar, R. K., and Kulshreshtha, S. C.: Glacier changes in the Garhwal Himalaya, India, from 1968 to 2006 based on remote sensing, J. Glaciol., 57, 543–556, 2011.

Bolch, T., Buchroithner, M., Pieczonka, T., and Kunert, A.: Planimetric and volumetric glacier changes in the Khumbu Himal, Nepal, since 1962 using Corona, Landsat TM and ASTER data, J. Glaciol., 54, 592–600, 2008.

Bolch, T., Kulkarni, A., Kääb, A., Huggel, C., Paul, F., Cogley, J. G., Frey, H., Kargel, J. S., Fujita, K., Scheel, M., Bajracharya, S., and Stoffel, F.: The state and fate of Himalayan glaciers, Science, 336, 310–314, 2012.

Brock, B., Mihalcea, C., Kirkbride, M., Diolaiuti, G., Cutler, M., and Smiraglia, C.: Meteorology and surface energy fluxes in the 2005–2007 ablation seasons at Miage debris-covered glacier, Mont Blanc Massif, Italian Alps, J. Geophys. Res., 115, D09106, doi:10.1029/2009JD013224, 2010.

Campbell, F. M. A., Nienow, P. W., and Purves, R. S.: Role of the supraglacial snowpack in mediating meltwater delivery to the glacier system as inferred from dye tracer investigations, Hydrol. Process., 20, 969–985, 2006.

TCD
9, 5373–5411, 2015

Carabelli: [Seismic survey 1957] Rilevamenti di ghiacciai e studi glaciologici in occasione dell'anno geofisico (Ghiacciaio del Miage): eslanazione geofisca, B. Comitato Glaciologico Italiano, 9, 87–94, 1961.
Casati, D.: Studio della dinamica di un debris-covered glacier: il Ghiacciaio del Miage, Tesi Laurea, Universita Milano, Milano, 1998.
Deline, P.: Etude géomorphologique des interactions entre écroulements rocheux et glaciers dans la haute montagne alpine: le versant sud-est du massif du Mont Blanc (Vallée d'Aoste, Italie), PhD Thesis, Université de Savoie, Chambéry, 2002.
Deline, P.: Interactions between rock avalanches and glaciers in the Mont Blanc massif during the late Holocene, Quaternary Sci. Rev., 28, 1070–1083, 2009.
Deline, P., Gardent, M., Kirkbride, M. P., Le Roy, M., and Martin, B.: Geomorphology and dynamics of supraglacial debris covers in the Western Alps, Geophys. Res. Abstr., 14, EGU2012-10866, 2012.
Dingman, S. L.: Physical Hydrology, 2nd Edn., Prentice Hall, New Jersey, 2002.
Diolaiuti, G., D'Agata, C., Meazza, A., Zanutta, A., and Smiraglia, C.: Recent (1975–2003) changes in the Miage debris-covered glacier tongue (Mont Blanc, Italy) from analysis of aerial photos and maps, Geogr. Fis. Din. Quat., 32, 117–127, 2009.
Flowers, G. E.: Subglacial modulation of the hydrograph from glacierized basins, Hydrol. Process., 22, 3903–3918, 2008.
Foster, L. A., Brock, B. W., Cutler, M. E. J., and Diotri, F.: A physically based method for estimating supraglacial debris thickness from thermal band remote sensing data, J. Glaciol., 58, 677–691, 2012.
Fountain, A. G.: Geometry and flow conditions of subglacial water at South Cascade Glacier, Washington State, USA; an analysis of tracer injections, J. Glaciol., 39, 143–156, 1993.
Fyffe, C. L.: The hydrology of debris-covered glaciers, PhD Thesis, University of Dundee, Dundee, 2012.
Fyffe, C. L., Reid, T. D., Brock, B. W., Kirkbride, M. P., Diolaiuti, G., Smiraglia, C., and Diotri, F.: A distributed energy-balance melt model of an alpine debris-covered glacier, J. Glaciol., 60, 587–602, 2014.
Gulley, J. and Benn, D. I.: Structural control of englacial drainage systems in Himalayan debris-covered glaciers, J. Glaciol., 53, 399–412, 2007.

TCD
9, 5373–5411, 2015

Gulley, J. D., Walthard, P., Martin, J., Banwell, A. F., Benn, D. I., and Catania, G.: Conduit roughness and dye-trace breakthrough curves: why slow velocity and high dispersivity may not reflect flow in distributed systems, J. Glaciol., 58, 915–925, 2012.
Hallet, B., Lorrain, R., and Souchez, R.: Rates of erosion and sediment evacuation by glaciers: a review of field data and their implications, Global Planet. Change, 12, 213–235, 1996.
Hasnain, S. I., Jose, P. G., Ahmad, S., and Negi, D. C.: Character of the subglacial drainage system in the ablation area of Dokriani glacier, India, as revealed by dye-tracer studies, J. Hydrol., 248, 216–223, 2001.
Hewitt, I. J. and Fowler, A. C.: Seasonal waves on glaciers, Hydrol. Process., 22, 3919–3930, 2008.
Hewitt, K.: Glaciers of the Karakoram Himalaya: Glacial Environments, Hazard and Resources, Springer, Dordrecht, 2014.
Hooke, R. LeB.: On the role of mechanical energy in maintaining subglacial water conduits at atmospheric pressure, J. Glaciol., 30, 280–287, 1984.
Hooke, R. LeB., Laumann, T., and Kohler, J.: Subglacial water pressures and the shape of subglacial conduits, J. Glaciol., 36, 67–71, 1990.
Hubbard, B. P., Sharp, M. J., Willis, I. C., Nielsen, M. K., and Smart, C. C.: Borehole water-level variations and the structure of the subglacial hydrological system of Haut Glacier d'Arolla, Valais, Switzerland, J. Glaciol., 41, 572–583, 1995.
Keinholz, C., Herreid, S., Rich, J. L., Arendt, A. A., Hock, R., and Burgess, E. W.: Derivation and analysis of a complete modern-date glacier inventory for Alaska and northwest Canada, J. Glaciol., 61, 403–420, 2015.
Kilpatrick, F. A. and Cobb, E. D.: Measurement of Discharge Using Tracers, United States Government Printing Office, Washington, 1985.
Kirkbride, M. P. and Deline, P.: The formation of supraglacial debris covers by primary dispersal from transverse englacial debris bands, Earth Surf. Proc. Land., 38, 1779–1792, 2013.
Kirkbride, M. P. and Dugmore, A. J.: Glaciological response to distal tephra fallout from the 1974 eruption of Heckla, south Iceland, J. Glaciol., 49, 420–428, 2003.
Lambrecht, A., Mayer, C., Hagg, W., Popovnin, V., Rezepkin, A., Lomidze, N., and Svanadze, D.: A comparison of glacier melt on debris-covered glaciers in the northern and southern Caucasus, The Cryosphere, 5, 525–538, doi:10.5194/tc-5-525-2011, 2011.

TCD
9, 5373–5411, 2015

Lejeune, Y., Bertrand, J- M., Wagnon, P., and Morin, S.: A physically-based model of the year-round surface energy and mass balance of debris-covered glaciers, J. Glaciol., 59, 327–344, 2013.

Lesca, C.: Emploi de la photogrammétrie analytique pour la determination de la vitesse supérficielle des glaciers et des profondeurs relatives, B. Comitato Glaciologico Italiano, 22, 169–186, 1974.

Mair, D., Nienow, P., Sharp, M. J., Wohlleben, T., and Willis, I.: Influence of subglacial drainage system evolution on glacial surface motion: Haut Glacier d'Arolla, Switzerland, J. Geophys. Res., 107, EPM 8-1–EPM 8-13, doi:10.1029/2001JB000514, 2002.

Maisch, M., Haeberli, W., Hoelzle, M., and Wenzel, J.: Occurrence of rocky and sedimentary glacier beds in the Swiss Alps as estimated from glacier-inventory data, Ann. Glaciol., 28, 231–235, 1999.

Mattson, L. E., Gardener, J. S., and Young, G. J.: Ablation on debris covered glaciers: an example from the Rakhiot Glacier, Punjab, Himalaya, IAHS-AISH P., 218, 289–296, 1993.

Maurya, A. S., Shah, M., Deshpande, R. D., Bhardwaj, R. M., Prasad, A., and Gupta, S. K.: Hydrograph separation and precipitation source identification using stable water isotopes and conductivity: River Ganga at Himalayan foothills, Hydrol. Process., 25, 1521–1530, 2011.

Nicholson, L. and Benn, D. I.: Calculating ice melt beneath a debris layer using meteorological data, J. Glaciol., 52, 463–470, 2006.

Nienow, P. W., Sharp, M., and Willis, I. C.: Velocity-discharge relationships derived from dye-tracer experiments in glacial meltwaters: implications for subglacial flow conditions, Hydrol. Process., 10, 1411–1426, 1996.

Nienow, P. W., Sharp, M., and Willis, I. C.: Seasonal changes in the morphology of the subglacial drainage system, Haut Glacier d'Arolla, Switzerland, Earth Surf. Proc. Land., 23, 825–843, 1998.

Oke, T. R.: Boundary Layer Climates, Methuen and Co. Ltd., London, 1978.

Østrem, G.: Ice melting under a thin layer of moraine, and the existence of ice cores in moraine ridges, Geogr. Ann., 41, 228–230, 1959.

Paterson, W. S. B.: The Physics of Glaciers, 3rd Edn., Butterworth-Heinemann, Oxford, 1994.

Pavan, M., Smiraglia, C., and Merlanti, F.: Prospezione Geofisca Sul Ghiacciaio Del Miage (Alpi Accidentali), Poster, Genova, 1999.

TCD
9, 5373–5411, 2015

Reid, T. D. and Brock, B. W.: Assessing ice-cliff backwasting and its contribution to total ablation of debris-covered Miage glacier, Mont Blanc massif, Italy, J. Glaciol., 60, 3–13, doi:10.3189/2014JoG13J045, 2014.
Röthlisberger, H.: Water pressure in intra- and subglacial channels, J. Glaciol., 11, 177–203, 1972.
Rounce, D. R. and McKinney, D. C.: Debris thickness of glaciers in the Everest area (Nepal Himalaya) derived from satellite imagery using a nonlinear energy balance model, The Cryosphere, 8, 1317–1329, doi:10.5194/tc-8-1317-2014, 2014.
Schauwecker, S., Rohrer, M., Huggel, C., Kulkarni, A., Ramanathan, AL., Salzmann, N., Stoffel, M., Thayyen, R. and Brock, B.: Remotely sensed debris thickness mapping of Bara Shigri Glacier, Indian Himalaya, J. Glaciol., 61, 675–688, 2015.
Scherler, D., Bookhagen, B., and Strecker, M. R.: Spatially variable response of Himalayan glaciers to climate change affected by debris cover, Nat. Geosci., 4, 156–159, 2011.
Schuler, T. V. and Fischer, U. H.: Modeling the diurnal variation of tracer transit velocity through a subglacial channel, J. Geophys. Res., 144, F04017, doi:10.1029/2008JF001238, 2009.
Seaberg, S. Z., Seaberg, J. Z., Hooke, R. LeB., and Wiberg, D. W.: Character of the englacial and subglacial drainage system in the lower part of the ablation area of Storglaciären, Sweden, as revealed by dye-trace studies, J. Glaciol., 34, 217–227, 1988.
Stokes, C. R., Popovnin, V., Aleyhikov, A., Gurney, S. D., and Shahgedanova, M: Recent glacier retreat in the Caucasus Mountains, Russia, and associated increase in supraglacial debris cover and supra-/proglacial lake development, Ann. Glaciol., 46, 195–203, 2007.
Willis, I. C., Sharp, M. J., and Richards, K. S.: Configuration of the drainage system of Midtdalsbreen, Norway, as indicated by dye-tracing experiments, J. Glaciol., 36, 89–101, 1990.
Willis, I. C., Arnold, N. S., and Brock, B. W.: Effect of snowpack removal on energy balance, melt and runoff in a small supraglacial catchment, Hydrol. Process., 16, 2721–2749, 2002.
Xu, J., Grumbine, R. E., Shrestha, A., Eriksson, M., Yang, X., Wang, Y., and Wilkes, A.: The melting Himalayas: cascading effects of climate change on water, biodiversity, and livelihoods, Conserv. Biol., 23, 520–530, 2009.

TCD
9, 5373–5411, 2015

Table 1. Details of supraglacial and proglacial stream instruments.

Quantity	Location	Time period	Manufacturer	Type	Accuracy
Stage	Proglacial	2010 and Jun 2011	GE Sensing	Druck PTX1830 (vented)	±0.1 % full scale (or ±0.06 % full scale)
	Proglacial	Aug and Sep 2011	Onset	HOBO U20-001-04 (non-vented)	±0.075 % full scale, ±0.3 cm
Fluorescence	Proglacial	2010 and Jun 2011	Seapoint	Rhodamine fluorometer	Not stated but minimum detection 0.02 ppb
	Proglacial	Jul, Aug, Sep 2011	Turner	Cyclops-7 Rhodamine	Not stated but minimum detection 0.01 ppb
Conductivity	Supraglacial	2010 and 2011	Hanna	HI9033 with HI 76302W probe	±1 % full scale (excluding probe)

TCD
9, 5373–5411, 2015

Table 2. Parameters calculated for each dye breakthrough curve.

Symbol	Unit	Definition
u	$m\,s^{-1}$	The minimum estimate of the average flow velocity (d/t).
d	m	The straight line distance from the gauging station to the injection site. Due to the bend in the glacier above S4, for all traces above this point the distance between the injection point and S4 was used and added to the distance between S4 and the gauging station to give the total distance.
t	s	The time between the injection and peak of the return curve.
D	$m^2\,s^{-1}$	The dispersion coefficient, which is a measure of the spread of the dye as it travels through the glacier, see Seaberg (1988, Eq. 4).
b	m	The dispersivity, calculated as D/u (Seaberg, 1988, p. 224).
A_m	m^2	The apparent mean cross-sectional area, calculated as Q_m/u.
Q_m	$m^3\,s^{-1}$	The mean discharge between the injection and detection point, calculated as the average of the supraglacial (assumed constant) and proglacial (average of the discharge at the injection and peak of the return curve) discharge.
V_r	mL	The volume of dye recovered, calculated from the equation below, which was derived from the equation to calculate discharge given by Kilpatrick and Cobb (1985, p. 6): $V_r = \frac{S^{-1}\left(\frac{1}{1.649\times10^{-8}}(Q_p A_c)\right)}{c_{di}}$
S	n/a	The specific gravity of the dye used (1.15 for rhodamine WT).
Q_p	$m^3\,s^{-1}$	The average proglacial discharge from the time of injection until the time of the peak of the dye return curve.
A_c	$ppb\,min^{-1}$	The area under the dye breakthrough curve.
c_{di}	ppb	The concentration of the dye prior to injection.
P_r	%	The percentage dye return ($(V_r/V_i) \times 100$).
V_i	mL	The volume of dye injected.

TCD
9, 5373–5411, 2015

Table 3. Mean supraglacial discharges (Q_s) and velocities (u_s) for the 2011 streams.

Name	Q_s ($m^3 s^{-1}$)	u_s ($m s^{-1}$)
S5	0.030	0.17
S7	0.019	0.24
S12	0.177	0.46
S14	0.622	1.52
S15	0.017	0.36

TCD
9, 5373–5411, 2015

Table 4. Dye trace parameters for all injection points in 2010, for definitions see Table 2. Mean P_r does not include values > 100 %.

Name	Date	V_i (mL)	Trace?	u ($m\,s^{-1}$)	D ($m^2\,s^{-1}$)	b (m)	Q_p ($m^3\,s^{-1}$)	A_c ($ppb\,min^{-1}$)	P_r (%)
S1	5 Jun 2010		N						
S2	8 Jun 2010	40	N						
S6	9 Jun 2010	40	Y	0.583	0.884	1.52	2.88	20.8	37.7
S8	10 Jun 2010	120	Y	0.434	1.180	2.72	2.90	55.9	34.0
S13	11 Jun 2010	200	Y	0.830	1.800	2.17	3.36	129.4	54.6
S1	12 Jun 2010	40	Y	0.024	0.004	0.15	5.97	34.4	129.0
S10	13 Jun 2010	160	Y	0.602	2.300	3.82	5.70	40.0	35.8
S3	14 Jun 2010	80	Y	0.192	0.230	1.20	2.84	3.7	3.3
S9	18 Jun 2010	120	N						
S3	19 Jun 2010	80	N						
S5	20 Jun 2010	80	N						
S3	29 Jul 2010	80	Y	0.345	0.860	2.49	10.71	50.6	170.0
S5	30 Jul 2010	120	Y	0.226	9.490	42.01	5.63	47.4	55.9
S9	31 Jul 2010	120	N						
S11	1 Aug 2010	120	Y	0.442	3.550	8.03	7.80	56.3	91.8
S13	3 Aug 2010	160	N						
S16	4 Aug 2010	200	N						
S5b	6 Aug 2010	80	Y*				2.98		
S13	5 Sep 2010	160	N						
S14b	6 Sep 2010	200	Y	0.613	1.770	2.89		181.9	
S3	9 Sep 2010	80	Y	0.265	1.870	7.05	1.65	100.2	51.9
S4	10 Sep 2010	80	N						
S12b	11 Sep 2010	100	Y	0.318	7.800	24.55	1.93	141.5	68.6
Mean (all)				0.406	2.645	8.21	4.63	71.8	48.2
Mean (upper)				0.561	3.444	8.29	4.74	109.8	62.7
Mean (lower)				0.296	2.074	8.16	4.57	44.7	36.6

* Only part of the rising limb of the trace was returned.

TCD
9, 5373–5411, 2015

Table 5. Dye trace parameters for all 2011 dye injections. The Q_s and u_s type is either "*D*", dilution gauging, "*V*", the velocity area method (timing of floats), or "AdD", adjusted to dilution gauging (see Sect. 3.1.2 for details). Means are for detected traces only and mean P_r does not include values > 100 %. Since the P_r for S_100911 exceeds 100 % this may indicate that the spikes on the tail of the main peak (Fig. 7b) are erroneous.

Name	Date	V_i (mL)	Trace?	u ($m\,s^{-1}$)	D ($m^2\,s^{-1}$)	b (m)	Q_p ($m^3\,s^{-1}$)	A_c (ppb min^{-1})	P_r (%)	Q_s ($m^3\,s^{-1}$)	Q_s type	u_s ($m\,s^{-1}$)	u_s type	A_m (m^2)
S7	5 Jun 2011	160	Y	0.073	2.907[a]	11.51[a]	2.14	70.1	23.5					
S5	6 Jun 2011	120	Y	0.070	14.70[a]	178.58[a]	2.08	83.9	36.6	0.027	D	0.24	D	14.68
S15	8 Jun 2011	280	N							0.027	D	0.44	D	
S14	9 Jun 2011	280	N							0.535	V	1.14	V	
S12	10 Jun 2011	280	Y	0.510	0.700	0.02	2.09	466.8	87.4	0.025	AdD	0.44	AdD	2.06
S7	11 Jun 2011	240	Y	0.124	2.070	3.88	2.01	124.0	26.1	0.011	AdD	0.17	AdD	8.14
S5	12 Jun 2011	200	Y	0.070	9.380[a]	113.82[a]	2.21	109.8	30.5	0.032	D	0.25	D	15.88
S15	13 Jun 2011	200	Y	0.283	71.400	144.08	3.00	123.1	46.3	0.013	D	0.27	D	5.36
S14	14 Jun 2011	200	Y	0.583	1.300	0.06	2.35	284.5	83.9	0.438	V	1.24	V	2.39
S3	15 Jun 2011	80	Y[b]											
S5	27 Jul 2011	200	Y	0.229	1.980	9.91	1.98	207.5	51.6	0.031	D	0.13	D	4.38
S15	28 Jul 2011	240	Y	0.439	1.570	0.22	2.85	196.4	58.6	0.010	D	0.27	D	3.25
S14	29 Jul 2011	160	Y	0.470	2.600	0.83	1.87	74.7	21.9	0.874[c]	V	2.13	V	2.92
S12	30 Jul 2011	160	Y	0.487	9.300	5.23	2.16	68.6	23.2	0.341	D	0.43	D	2.56
S7	31 Jul 2011	200	N							0.028	D	0.24	D	
S14	1 Aug 2011	120	Y	0.731	1.240	0.26	4.47	41.0	38.3	0.888[c]	V	2.16	V	3.66
S15	1 Aug 2011	120	Y	0.576	1.230	0.35	4.47	42.9	40.1	0.014	D	0.30	D	3.89
S12	2 Aug 2011	160	Y	0.699	1.440	0.22	4.47	69.7	48.8	0.147	AdD	0.50	D	3.30
S7	3 Aug 2011	190	N							0.032	D	0.28	D	
S5	4 Aug 2011	195	N							0.028	D	0.14	D	
S5	12 Sep 2011	200	Y	0.063	0.09[a]	1.16[a]	7.22	179.9	163.0					
S15	13 Sep 2011	240	Y	0.578	4.50	0.47	5.16	134.6	72.6	0.022	D	0.50	D	4.43
S14	14 Sep 2011	120	Y	0.697	1.40	0.27	6.02	45.0	56.6	0.378[c]	V	0.92	V	4.60
S12	14 Sep 2011	160	Y	0.593	3.54	1.16	6.34	71.4	71.0	0.196	D	0.49	D	5.54
S7	15 Sep 2011	200	Y	0.107	49.98	68.81	4.53	164.5	93.5	0.006	D	0.25	D	22.31
Mean (all)				0.389	9.54	28.47	3.55	134.6	50.6	0.203		0.63		6.43
Mean (upper)				0.554	8.35	12.76	3.77	134.9	54.1	0.279		0.80		3.66
Mean (lower)				0.105	11.59	55.38	3.17	134.2	43.6	0.022		0.21		13.08

[a] Indicates traces with multiple peaks for which the *D* and *b* parameters are less reliable.
[b] Only the first part of the trace was returned.
[c] The Q_s values are an estimate because the stream cross-sectional area could not be measured, in these cases the mean cross-sectional area was multiplied by the velocity.

TCD
9, 5373–5411, 2015

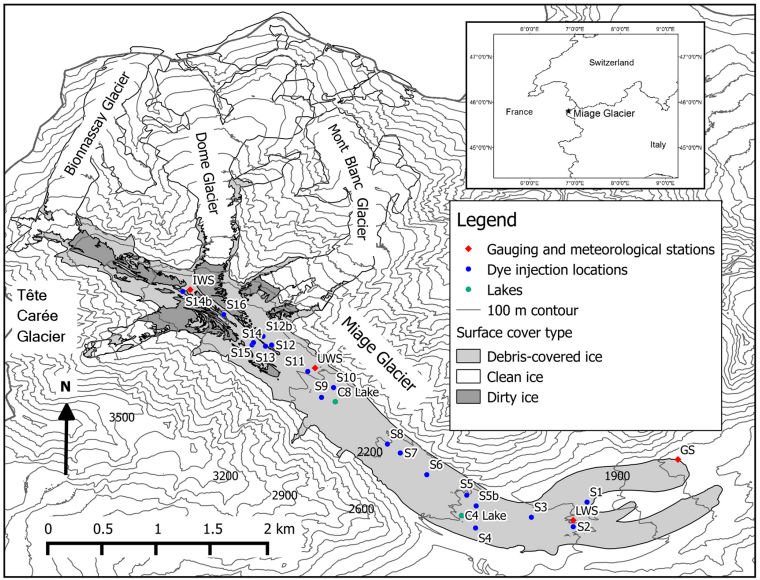

Figure 1. Map of Miage Glacier showing location of monitoring stations, lakes and dye tracing points. Inset shows location of Miage Glacier in the Alps. "IWS" is the ice weather station, "UWS" the upper weather station, "LWS" the lower weather station and "GS" the gauging station.

TCD
9, 5373–5411, 2015

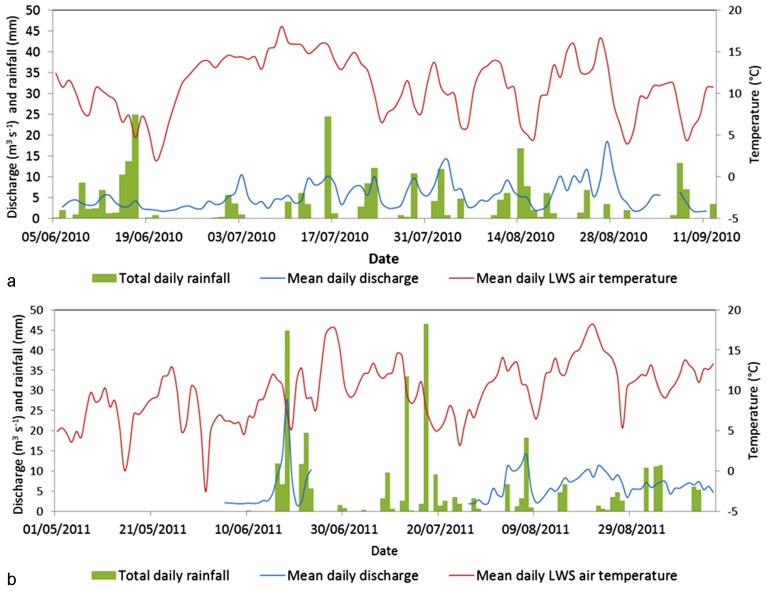

Figure 2. Meteorological conditions and discharge during the **(a)** 2010 and **(b)** 2011 field seasons.

TCD
9, 5373–5411, 2015

Figure 3. (a) The englacial conduit above the S8 stream, **(b)** dye tracing the S12 stream in September 2011 and **(c)** dye tracing S14 in July 2011.

TCD
9, 5373–5411, 2015

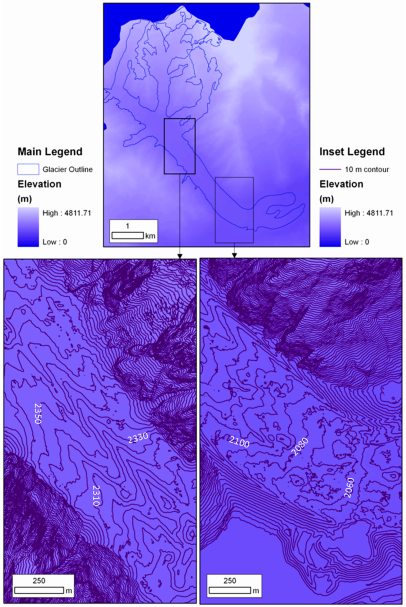

Figure 4. Topographic influence on supraglacial hydrology. The top panel gives an overview of catchment topography. The left inset shows the clear along-glacier ridge and valley topography associated with the central, eastern and western moraines on the upper tongue. The right inset shows hummocky topography on the lower glacier. Both insets show contours at 10 m intervals. Source: Regione Autonoma Valle d'Aosta DEM.

TCD
9, 5373–5411, 2015

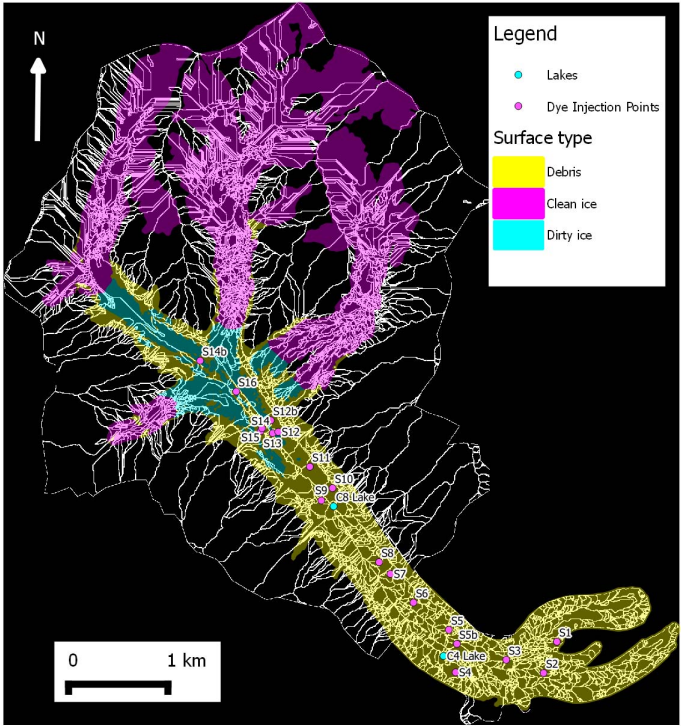

Figure 5. A map of the outlines (shown as white lines) of the modelled supraglacial catchments.

TCD
9, 5373–5411, 2015

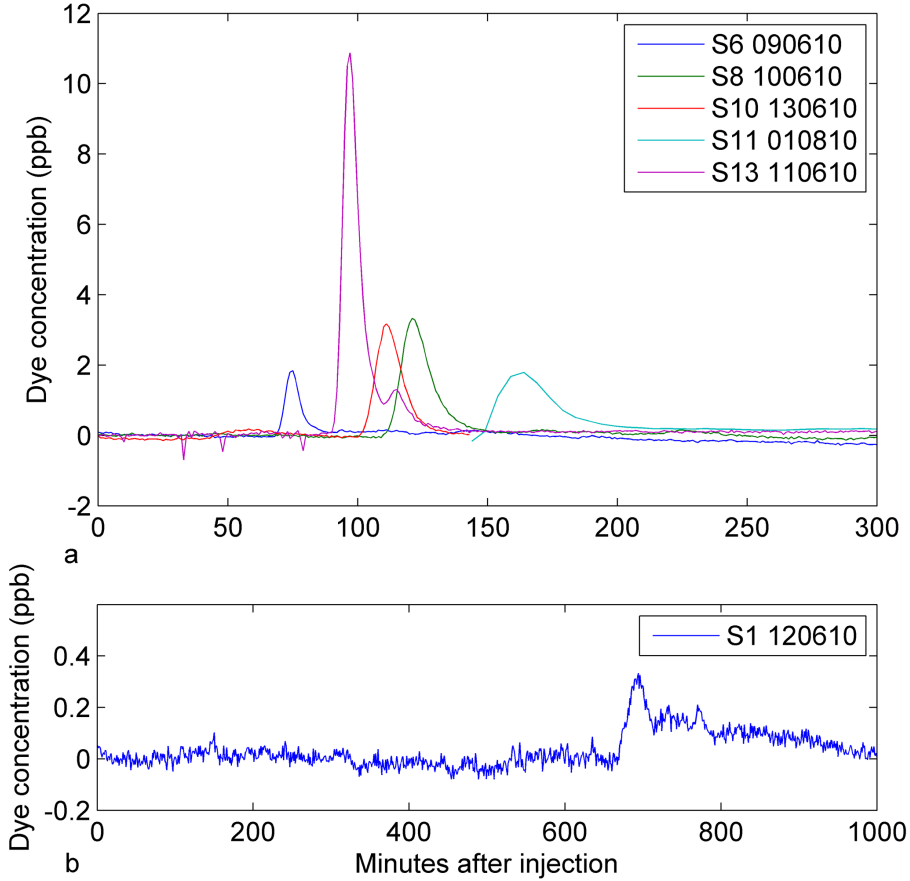

Figure 6. Dye return curves from streams that were only traced once. Note that vertical and horizontal scales differ between subplots.

TCD
9, 5373–5411, 2015

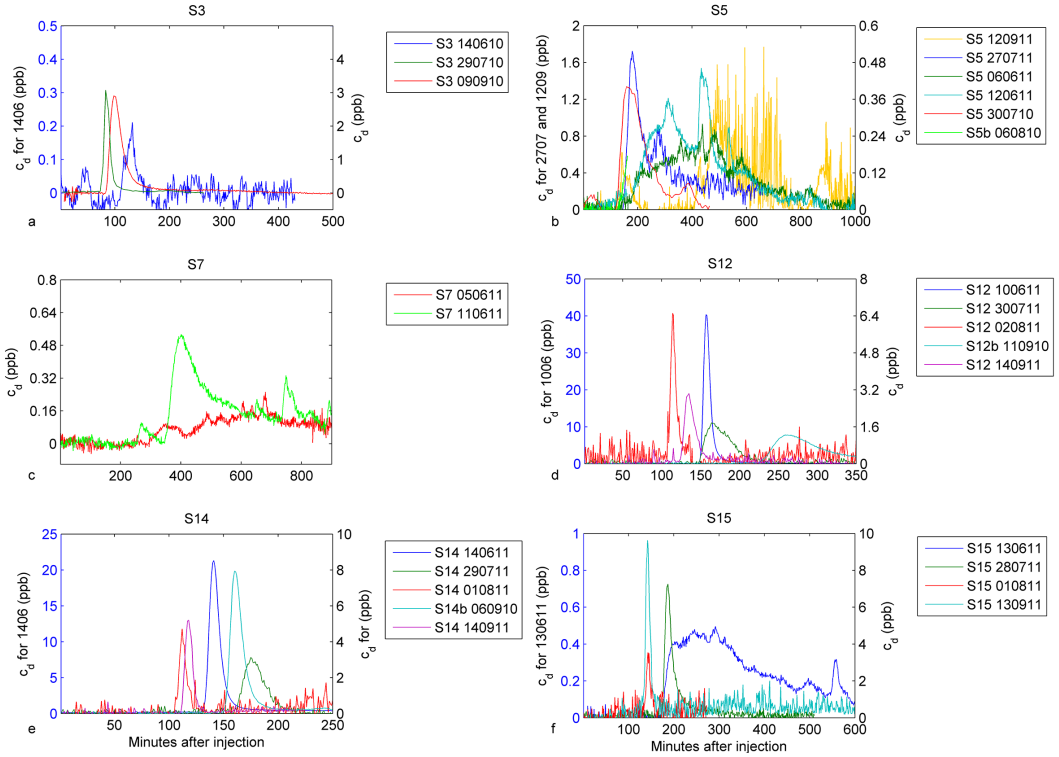

Figure 7. Repeat dye return curves from single injection points, where c_d is the dye concentration. The injection points S3, S5 and S7 **(a, b, c)** are on the lower glacier, while injection points S12, S14 and S15 **(d, e, f)** are on the upper glacier. Note that vertical and horizontal scales differ.

TCD
9, 5373–5411, 2015

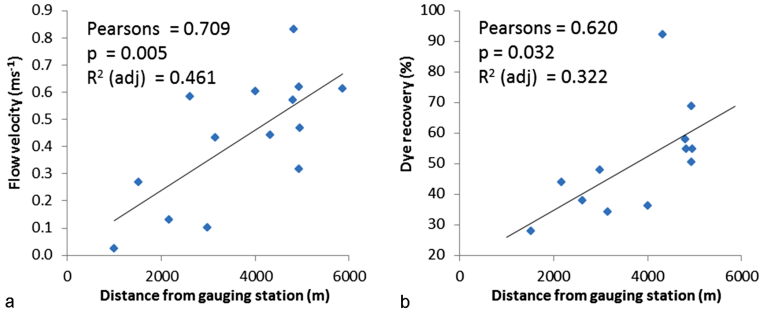

Figure 8. Relationship between the distance to gauging station and **(a)** average injection point u, and **(b)** average injection point P_r, including all 2010 and 2011 data. P_r in **(b)** does not include values over 100 %.

TCD
9, 5373–5411, 2015

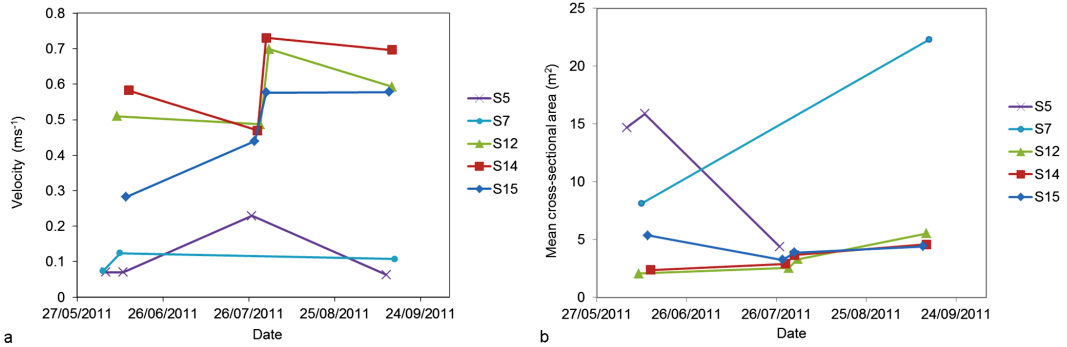

Figure 9. (a) Dye trace u variations over the 2011 season, and **(b)** mean A_m variations over the 2011 season.

TCD
9, 5373–5411, 2015